Boundary Layer Evolution within a Canyonland Basin. Part I: Mass, Heat, and Moisture Budgets from Observations

C. DAVID WHITEMAN

Pacific Northwest National Laboratory, Richland, Washington

THOMAS B. MCKEE

Colorado State University, Fort Collins, Colorado

J. C. DORAN

Pacific Northwest National Laboratory, Richland, Washington

(Manuscript received 11 December 1995, in final form 3 June 1996)

ABSTRACT

Individual terms of the mass, heat, and moisture budget equations are evaluated for an atmospheric control volume in Colorado's Sinbad Basin using tethered balloon and surface energy budget data obtained during a 16.5-h period on 15–16 July 1988. The basin was chosen for its simple topography and arid climate, which simplified the evaluation of some of the budget terms. The paper documents the many assumptions that are required to evaluate the mass, heat, and moisture budget equations in confined terrain using small datasets.

The nighttime outflow of air from the basin produced a compensatory mean sinking motion of 0.026 m s^{-1} at the top of the basin control volume and brought warm air into the top of the basin atmosphere. In contrast to previous reports for well-drained valleys, a high rate of atmospheric cooling continued in this basin throughout the entire night. The cooling is attributed primarily to turbulent sensible heat flux divergence and, to a lesser extent, radiative flux divergence. Measured sensible heat fluxes on the basin floor were small, suggesting that downward turbulent sensible heat fluxes must be relatively stronger in the downslope flows that develop above the sidewalls.

A general means of characterizing and comparing the energetics of basin and valley atmospheres is developed from the heat budget equation and is illustrated using data from other valleys and basins.

An accompanying paper takes a complementary approach of evaluating the heat budget terms using a dynamic model.

1. Introduction

In recent years a number of investigators have evaluated components of atmospheric mass, heat, and moisture budgets in valleys and basins. The focus of these experiments has been to determine the thermal forcing of the local circulations and the sources of air that support these flows. Such experiments have been conducted for Colorado's Brush Creek Valley (Whiteman and Barr 1986; Vergeiner et al. 1987; Horst et al. 1987, 1989), Austria's Inn Valley (Freytag 1985, 1987), Switzerland's Dischma Valley (Hennemuth and Köhler 1984; Hennemuth 1985, 1986), Japan's Aizu Basin (Kondo et al. 1989), and Japan's Akaigawa Basin (Maki et al. 1986). These investigations, by and large, have been exploratory experiments in which individual budget terms were evaluated from observational data under stated assumptions, with key terms calculated as residuals. Significant heat budget imbalances are a feature of experiments in which terms were independently evaluated, and recent lidar and tethersonde observations in valleys have suggested that along-valley and vertical advection terms are especially difficult to evaluate in complex terrain situations.

In this two-part article, we calculate budget components for an isolated canyonland basin where the topographic situation and climate produce significant budget simplifications. In Part I we evaluate the individual terms of the mass, heat, and moisture budgets for this basin using observational data. We call attention to the assumptions required to obtain the terms in the budget and point out the uncertainties arising in our work and in that of previous investigators from these assumptions and from limitations in the data. In Part II (Fast et al. 1996) we take an alternative approach of simulating the evolution of temperature and wind structure in the basin with a mesoscale numerical model.

Corresponding author address: Dr. C. David Whiteman, Pacific Northwest National Laboratory, P.O. Box 999, Richland, WA 99352. E-mail: cd_whiteman@pnl.gov

© 1996 American Meteorological Society

With this approach, budget balances are necessarily maintained at all times by the model equations. The model outputs are then postprocessed to compute the roles of the individual terms of the heat budget equation, to evaluate the validity of the assumptions used in the data analysis, and to examine conclusions drawn from that analysis.

Section 2 of this paper presents the mass, heat, and moisture budget equations for an atmospheric volume. In section 3 we discuss the approach used to evaluate these equations for an atmospheric control volume in Colorado's arid Sinbad Basin using data collected there in July 1988. To facilitate this evaluation we present information on the basin topography, the synoptic environment of the experiments, and the measurements. Sections 4–6 provide evaluations of individual terms of the mass, heat, and moisture budgets, respectively, using measurement data. This is followed, in section 7, by further discussions of the results of the budget evaluations. Conclusions are drawn in section 8.

2. Atmospheric mass, heat, and moisture budgets

We begin by presenting equations for the atmospheric mass, heat, and humidity budgets for an atmospheric volume.

a. Mass budget

The integral form of the mass continuity equation is

$$\iiint \frac{\partial \rho}{\partial t}\, dv + \iint \rho \mathbf{V}\cdot\mathbf{n}\, dA = 0 \quad (\text{kg s}^{-1}), \quad (1)$$

where ρ is atmospheric density, t is time, v is volume, $\mathbf{V}$ is the velocity vector, and $\mathbf{n}$ is the unit vector normal to an infinitesimal element of surface area dA and is directed out of the volume. The equation states that changes in atmospheric mass within a volume arise from differential mass fluxes across the volume boundaries.

b. Heat budget

By logarithmically differentiating Poisson's equation and combining it with the first law of thermodynamics, we can obtain the equation

$$dh = c_p \frac{T}{\theta}\, d\theta \quad (\text{J kg}^{-1}), \quad (2)$$

where c_p is specific heat at constant pressure, T is temperature, and $d\theta$ is the change in potential temperature caused by adding an increment of heat dh to a unit mass of air. The equation states that the potential temperature of a parcel of air is conserved under adiabatic conditions. After multiplying (2) by the air density, differentiating with respect to time, expanding the total differential, Reynolds averaging, and assuming that radiative flux divergence is the only diabatic process to be considered, we arrive at the equation

$$\bar{\rho} c_p \left[\frac{\partial \bar{\theta}}{\partial t} + \nabla\cdot(\bar{\mathbf{V}}\bar{\theta}) + \nabla\cdot(\overline{\mathbf{V}'\theta'}) \right] = -\frac{\theta}{T}\nabla\cdot\bar{\mathbf{R}} \quad (\text{W m}^{-3}), \quad (3)$$

where $\mathbf{R}$ is the vector net all-wave radiation, and the overbars represent an ensemble average. The factor θ/T, which has a value near one, is often neglected. Integrating over volume results in the atmospheric heat budget equation

$$\underbrace{\iiint \bar{\rho} c_p \frac{\partial \bar{\theta}}{\partial t}\, dv}_{\text{A}} = \underbrace{\iiint -\bar{\rho} c_p \nabla\cdot(\bar{\mathbf{V}}\bar{\theta})\, dv}_{\text{B}} + \underbrace{\iiint -\left(\frac{\theta}{T}\right)\nabla\cdot\bar{\mathbf{R}}\, dv}_{\text{C}} + \underbrace{\iiint -\bar{\rho} c_p \nabla\cdot(\overline{\mathbf{V}'\theta'})\, dv}_{\text{D}} \quad (\text{W}), \quad (4)$$

which specifies that the rate of increase of heat storage in an atmospheric volume (term A) depends on the convergence of potential temperature flux by the mean wind (term B), the convergence of radiative flux (term C), and the convergence of turbulent sensible heat flux (term D) into the atmospheric volume.

c. Moisture budget

A derivation analogous to that above for (4) (see, e.g., Hennemuth and Neureither 1986) results in the atmospheric moisture budget equation

$$\iiint \bar{\rho} \frac{\partial \bar{q}}{\partial t}\, dv = \iiint -\bar{\rho}\nabla\cdot(\bar{\mathbf{V}}\bar{q})\, dv + \iiint -\bar{\rho}\nabla\cdot(\overline{\mathbf{V}'q'})\, dv \quad (\text{kg s}^{-1}), \quad (5)$$

where q (kg kg^{-1}) is specific humidity. This equation specifies that the rate of increase of water vapor storage in an atmospheric volume depends on the convergence of moisture flux into the volume by the mean wind and the convergence of turbulent moisture flux. Note that (5), if multiplied by the latent heat of vaporization, would express the latent heat budget of the atmospheric volume.

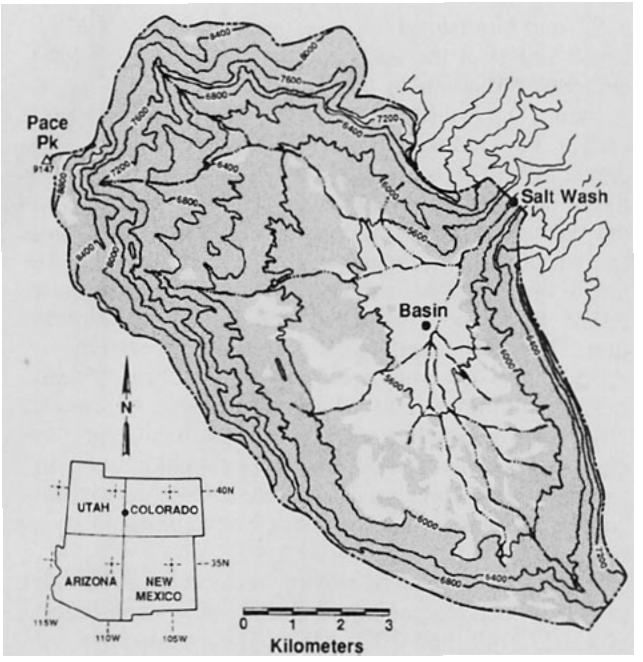

FIG. 1. Topographic map of the Sinbad Basin, Colorado, experimental area. The contour interval is 400 ft (122 m). The two observation sites are indicated with heavy dots. The stippling indicates the areas of the basin covered with forest or shrub vegetation.

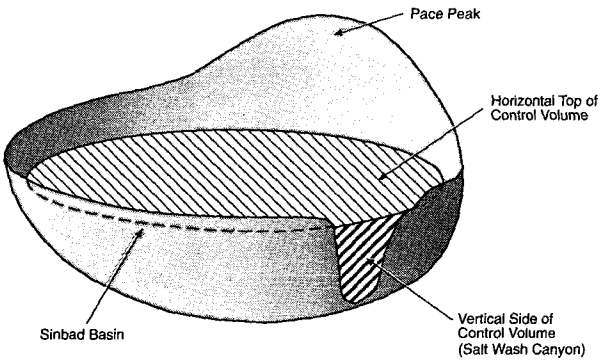

FIG. 2. Schematic diagram of the Sinbad Basin control volume.

3. Experimental design

In this section we discuss the basin topography, the synoptic weather conditions during the experiment, the observations to be used in evaluating the budget equations, and the methodology.

a. The Sinbad Basin

The Sinbad Basin (Fig. 1) is an elliptical basin formed from the collapse of an anticline that was underlain by a salt dome (Barnes 1978). Because the basin formed on the crest of an anticline, the basin has sharp ridgeline boundaries and practically no drainage area above the red sandstone cliffs that form the upper sidewalls. The basin has only one exit, the deep and narrow Salt Wash Canyon. This narrow canyon was expected to restrict the flow of air into and out of the basin so that the basin atmosphere would be relatively isolated and quiescent. Further, the arid climate would reduce latent heat fluxes within the basin. Since there are no extensive elevated drainage areas feeding the basin, the basin was expected to be isolated from upper-air influences, at least under weak upper-air flows.

The experiment was designed to evaluate the mass and heat budgets for a fixed atmospheric control volume in Colorado's Sinbad Basin, as shown schematically in Fig. 2. The lower boundary of the control volume is the basin floor and sidewalls, the upper boundary is a horizontal surface at some height h within the basin, and the control volume is closed by a vertical surface extending across the exit canyon from sidewall to sidewall. The control volume is defined in this way to simplify the advection terms in the budget equations since air can enter or exit the control volume only through two surfaces—the horizontal lid of the control volume and the vertical cross section through the exit canyon.

Relevant topographical characteristics of the basin are summarized in Figs. 3, 4, and 5, as obtained from the 7.5-min series of topographic maps (contour intervals—20 and 40 ft). Areas were obtained by planimeter. Figure 3 shows ridgetop elevation as a function of distance along the ridge crest, as measured clockwise around the basin. The Salt Wash Canyon is the only low-elevation opening in the basin topography. There are two small saddles on the south and southeast boundaries of the basin, but the airshed is generally closed below an elevation of about 2214 m above mean sea level (MSL), which is taken to be the height of the control volume lid, h. The north and west sides of the basin rise above the control volume lid and culminate in Pace Peak at 2800 m MSL. Figure 4 shows the drainage area and the cumulative volume of the basin as a function of height. Where area or volume computations are made for heights above the confined basin, the

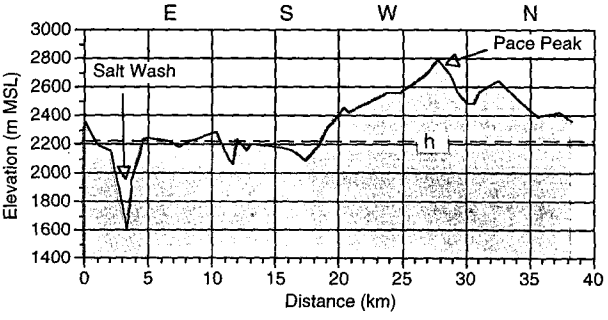

FIG. 3. Ridge crest elevation as a function of distance around the basin periphery.

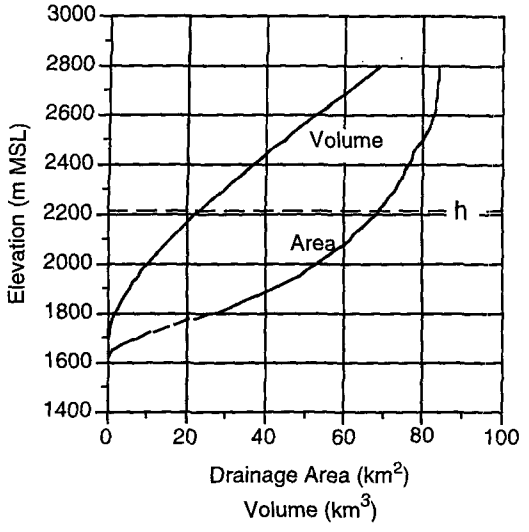

FIG. 4. Basin drainage area and cumulative volume as a function of elevation.

ridgeline is considered to be the horizontal boundary of the basin. The total drainage area of the basin is 83.8 km^2. The area of the control volume lid is $A_{xy}(h)$ = 69.3 km^2, and the volume is $v(h)$ = 23.8 km^3. Figure 5 presents the cumulative cross-sectional area of the Salt Wash Canyon as a function of elevation. The lowest 400 m of the canyon are quite narrow, but the canyon cross section increases rapidly above this height. The area of the vertical control volume surface through the canyon is $A_{yz}(h)$ = 0.70 km^2. The topography of the basin suggests that air cooled in the basin at night, if not drained out the Salt Wash Canyon, will accumulate within the basin to height h before beginning to spill out the south end of the basin.

b. Synoptic environment of the experiments

Experiments in the Sinbad Basin were performed during a 16.5-h experimental period beginning at 1800 mountain standard time (MST) 15 July 1988. A weak cold front passed south through the area in the early afternoon of 15 July. With the frontal passage, a narrow rain shaft crossed the south end of the basin but produced no rain at the experimental sites. After the frontal passage, synoptic-scale pressure patterns were weak and disorganized. High thin cirrus clouds persisted during the entire experimental period, although sky coverage was variable.

c. Meteorological and soil observations in the basin

Meteorological data were collected at two sites in the basin (Fig. 1), the basin site (38°30′52″N, 108°59′14″W, 1664 m MSL) and the Salt Wash site (38°32′09″N, 108°58′05″W, 1572 m MSL). For reference, astronomical sunset on 15 July occurred at 1936 MST and sunrise on 16 July occurred at 0509 MST. Local sunset at the basin site occurred at 1855 MST because of shading by the west sidewall.

Identical Atmospheric Instrumentation Research (AIR), Inc., model TS-3A-SP Tethersondes® were operated from the basin and Salt Wash sites, and free-flying model AS-1 AIR Airsondes® were released from the basin site. The Tethersondes have published precisions of ±0.5°C for the dry- and wet-bulb temperature sensors, ±5% for humidity, ±1 mb for pressure, ±0.25 m s^{-1} for wind speed, and ±5° for wind direction. The Airsondes have published precisions of ±0.5°C for dry- and wet-bulb temperature sensors, ±3% for humidity, and ±3 mb for pressure. AIR model HB-1A reference barometers and Assmann-type psychrometers were used before each tethered balloon and free-flying balloon launch to set the sonde surface pressure and to verify that the sondes were working properly.

At the basin site, free-flying meteorological sondes provided deep temperature, humidity, and wind profiles at 1802, 2147, and 1020 MST. These soundings (not shown) indicated that winds above the basin during the experimental period were generally weak and variable in direction. The 1802 sounding showed a convective boundary layer (CBL) above the basin floor to an altitude of 2700 m MSL. Winds were from the southwest at about 5 m s^{-1} to heights of 3200 m MSL. By 2147 the entire depth of the afternoon CBL had cooled, but cooling was especially strong within the lowest 250 m of the basin. Winds had become weak within the basin temperature inversion. Above the inversion the winds were variable in direction but in some elevated layers attained speeds up to 8 m s^{-1}. The 1020 sounding was taken at the conclusion of the basin temperature breakup period on 16 July and showed a 750-m-deep convective boundary

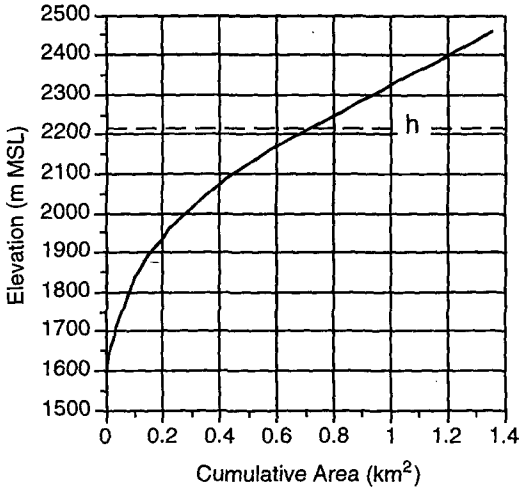

FIG. 5. Cumulative vertical cross-sectional area across the Salt Wash Canyon as a function of elevation.

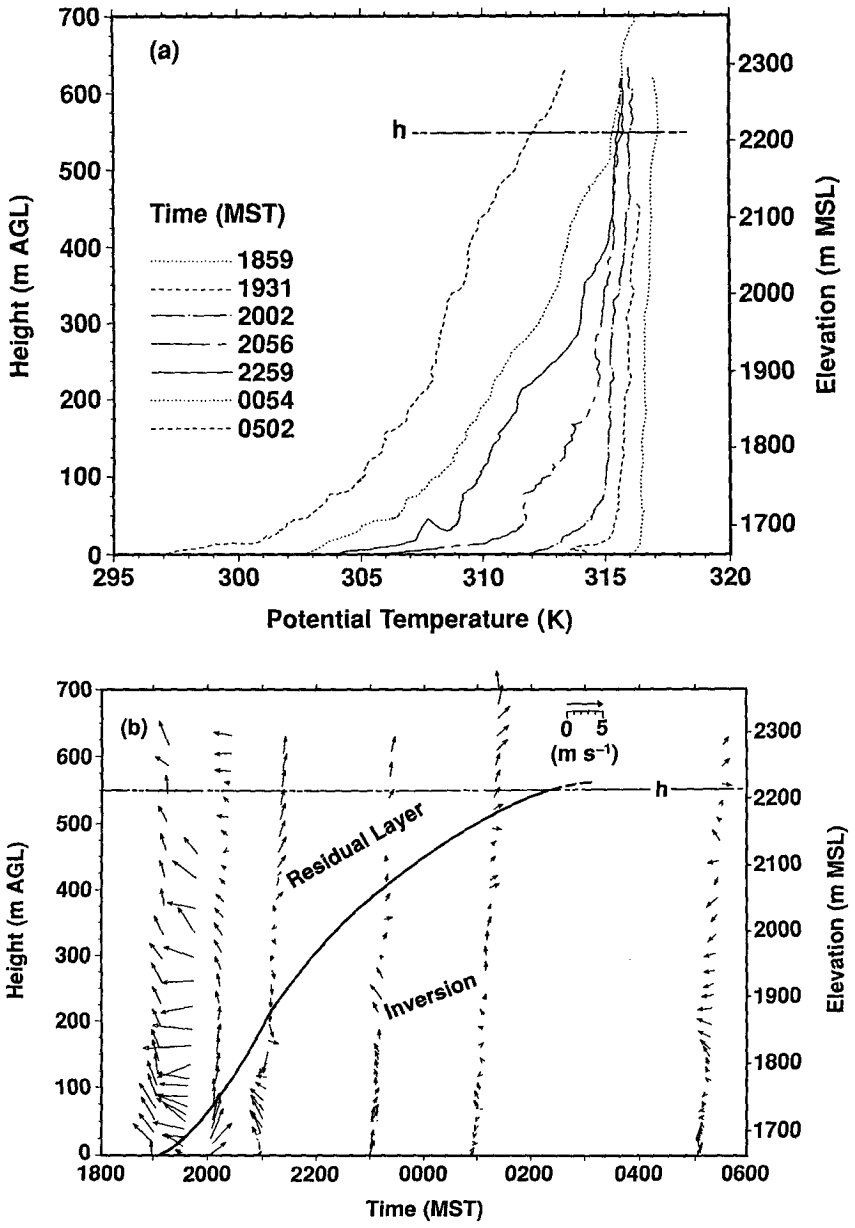

FIG. 6. Tethered balloon profiles of (a) potential temperature and (b) winds at the basin site during the period of evening and nighttime cooling on 15–16 July 1988.

layer over the floor of the basin. Winds were variable in direction, with speeds up to 4 m s^{-1}. A cooling of less than 1°C occurred above the basin to altitudes of 3200 m MSL between the 2147 and 1020 soundings. The weak flows and small changes in temperature profiles above the basin show that the basin was isolated from large-scale influences during the experiment.

Tethered balloon sondes provided detailed periodic temperature, humidity, and wind soundings to altitudes of about 700 m above ground level (AGL). During the evening and nighttime cooling period (Fig. 6a), the basin atmosphere cooled strongly despite variable thin cirrus clouds. Initially, cooling occurred rather uniformly through the basin depth, but after the 2056 MST sounding most of the cooling was confined to the growing surface-based stable layer that began to form at about 1900 MST. The potential temperature inversion deepened through the night until, after 0100 MST, it reached the level of the lowest ridges. Strong cooling of the whole basin atmosphere then continued until sunrise. Winds (Fig. 6b) became weak within the developing stable boundary layer.

Initially, because of afternoon convective mixing, there was little variation of specific humidity with height in the basin, with values of about 7.2 g kg^{-1} (humidity soundings are not shown in the figures). After the surface-based inversion began to form, however, humidity increased through the basin depth, with highest humidities measured near the ground, suggesting that it was the humidity source. The basin atmosphere, however, began to dry after about 2100 MST, with initial drying at the upper levels. By sunrise, the entire basin atmosphere had dried, with specific humidities of 6.5–7 g kg^{-1} through the bulk of the basin atmosphere.

After sunrise (Fig. 7a), the basin atmosphere began to warm as a convective boundary layer grew upward from the surface. Warming occurred primarily within, but also above, the growing convective boundary layer. Light and variable winds (Fig. 7b) persisted within the basin during the warming period. Specific humidities became nearly constant with height within the growing convective boundary layer and increased to 7.5 g kg^{-1} by the final sounding.

Tethered balloon soundings were also made from the center of the canyon floor at the Salt Wash site. There hourly soundings were made during the period from 1900 to 0200 MST to measure temperature (Fig. 8a) and humidity profiles in the canyon and to determine the strength of the canyon winds (Fig. 8b). The Salt Wash tethered balloon system was identical to the one used at the basin site, and a field intercomparison of the two sondes indicated that temperatures agreed to within 0.1 K, so that no calibration corrections were necessary. Temperature profiles in the canyon are similar to those in the basin at the same AGL heights (compare Figs. 8a and 6a), except for unsteadiness in the small-scale vertical structure and a tendency toward neutral stability in well-mixed air in the lowest 50–75 m of the canyon. This temperature profile similarity shows that the canyon is simply serving as a conduit for air being advected out of the basin. Winds in the canyon were turbulent in the early evening, and a short-lived wind reversal in the lower part of the canyon occurred in the 1915 MST sounding. Once the basin inversion formed, the winds blew down the axis of the canyon, generally at speeds of 4–7 m s^{-1}.

In addition to the atmospheric soundings, measurements of soil temperatures and net radiation were made at the basin site. Epoxy-potted copper-constantan thermocouples were used for the temperature measurements (precision ± 0.2°C), and a Fritschen miniature net radiometer was used for the radiation measurements. Data were sampled at 5-s intervals with a Campbell Scientific, Inc., CR-21X data collection system, and 5-min averages were recorded. Six thermocouples were buried at depths of 0.00, 0.05, 0.11, 0.24, 0.50, and 1.05 m to provide soil temperature profiles (Fig. 9) under a sparse cover of cheatgrass on a homogeneous sandy soil alluvium. The thermocouples were installed horizontally in undisturbed soil through the vertical south wall of a soil pit dug and backfilled on 12 July. The soil thermocouple at a nominal depth of 0.00 m was actually inserted under a thin layer of surface litter so that it could not be directly affected by insolation or longwave radiative equilibrium with the sky. Seven soil samples were collected at selected depths when the pits were dug. A single sample of the top 2 cm of soil collected at the conclusion of the experiments on 17 July showed no significant change in soil moisture status since 12 July. The net radiometer was exposed over an undisturbed soil surface at a height of 1.54 m. Nighttime net radiometer data were multiplied by a factor of 1.37 following a suggestion by the designer/manufacturer (L. J. Fritschen 1989, personal communication) to account for a known nighttime undermeasurement of net radiation caused by the differing response of the transducer to long- and shortwave radiation. His suggestion was based on calibration of a similar model radiometer in a hemispherical chamber where the long- and shortwave radiation were independently varied.

d. Method

Tethered balloon potential temperature and humidity profiles were obtained approximately every hour at the Salt Wash site and at variable intervals at the Sinbad Basin site. The first step in the processing was to average each sounding over 25-m intervals from the surface to the control volume lid (i.e., to 550 m AGL at the Sinbad site and to 650 m AGL at the Salt Wash site). All vertical integrals were subsequently approximated by sums over these 25-m-deep layers. Consecutive pairs of layer-averaged soundings at the Sinbad site were then used to determine time-interpolated layer-averaged soundings at the Sinbad site valid for the same times as the Salt Wash soundings. Changes of atmospheric heat and moisture storage in the control volume and fluxes of mass, heat, and moisture across control volume surfaces were then calculated as averages over the hourly intervals between sounding times. Note that two of the Salt Wash soundings did not attain the lid height (Fig. 8a); winds, temperatures, and humidities at the upper levels of these soundings were interpolated linearly between the last-measured values at the tops of the soundings and time-interpolated values at the lid height. The Salt Wash soundings ended with the 0100 MST sounding when the basin inversion approached the top of the basin control volume. Calculated values of selected parameters after the Salt Wash soundings ended were averaged over the variable time intervals of the successive Sinbad Basin soundings.

Individual control volume heat budget terms, from (4), are expressed in watts. After calculation, these terms were normalized by dividing by the area of the control volume lid. They are thus reported in units of watts per square meter. This has several advantages. First, the numerical values are comparable in magnitude to the surface fluxes

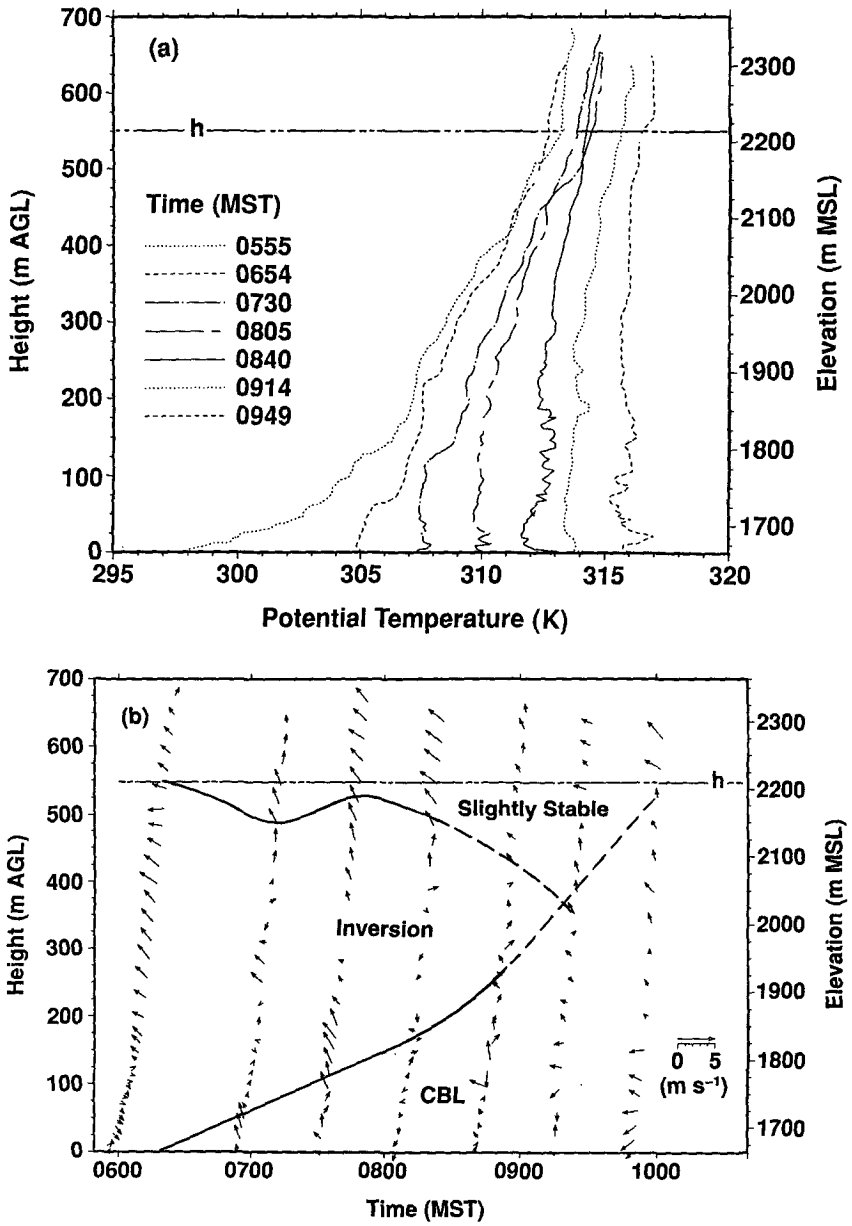

FIG. 7. Tethered balloon profiles of (a) potential temperature and (b) winds at the basin site during the period of daytime warming on 16 July 1988.

with which most researchers are familiar. Second, the divergence theorem allows us to evaluate flux divergences in terms of differences in fluxes through the surfaces of the control volume, so that there is a mathematical basis for the units. Third, this construct provides a means of comparing heat budget terms obtained in valleys of different volumes. Finally, the construct has a physical basis in that major sources of energy (radiation and advection) driving the basin heat budget come through the area at the top of the basin.

4. Evaluation of the basin atmospheric mass budget

Local changes of density within the basin control volume were assumed negligible during the 1-h averaging period, so (1) reduces to a statement that the mass flowing horizontally out of the control volume through the Salt Wash Canyon is balanced by the mass flowing vertically into the volume through the horizontal control volume lid, as follows:

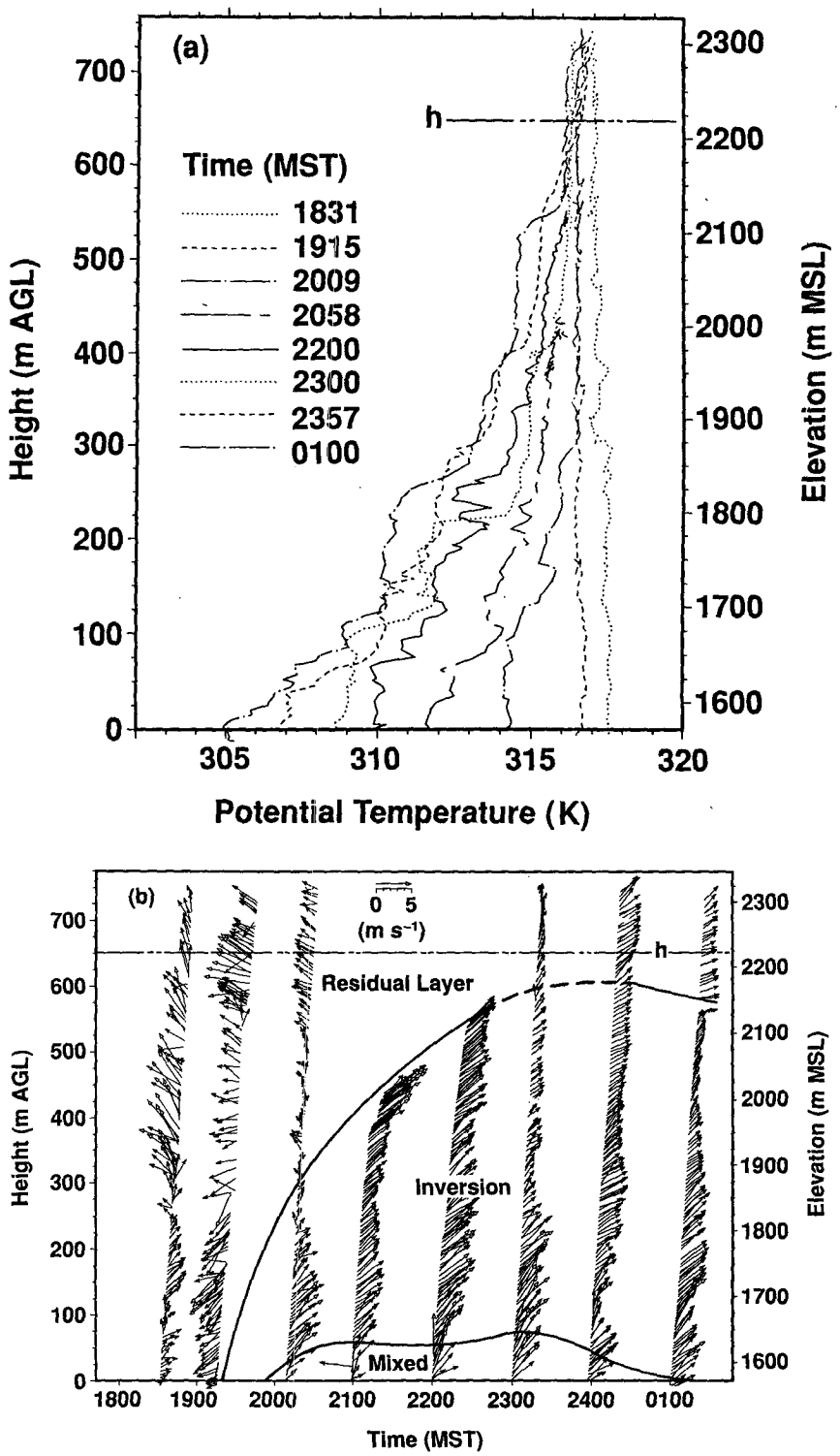

FIG. 8. Tethered balloon profiles of (a) potential temperature and (b) winds at the Salt Wash Canyon site during the period of evening and nighttime cooling on 15–16 July 1988.

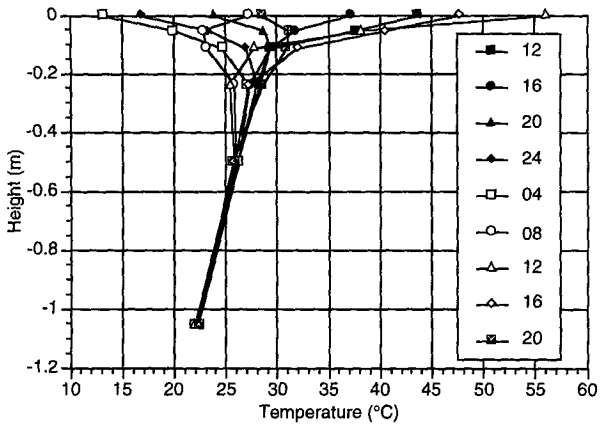

FIG. 9. Soil temperature profiles at the basin site at different times of day (MST) on 15–16 July 1988.

$$\int \rho(z) a u_c(z) b(z) dz + \langle \rho w \rangle_h A_{xy}(h) = 0 \quad (\text{kg s}^{-1}), \tag{6}$$

where u_c is the horizontal down-canyon wind speed component over the valley center, a is a dimensionless factor that is applied to u_c to obtain a wind speed representative of the canyon width, b is the canyon width, w is the vertical velocity, and angle brackets represent an average over the control volume lid.

The neglect of the first term in (1), the local rate of change of density in the volume, is justified by its small value. This term averages 0.015 metric tons per second (ton s^{-1}) in the evening and is only 0.9% of each of the remaining terms.

The factor a in (6) is less than 1 since the wind speed decreases as the sidewalls are approached. The numerical value used (0.7) was derived by Clements et al. (1989) using Doppler lidar and tethered balloon data in Colorado's Brush Creek Valley. They noted that their numerical value differs slightly from the theoretical value of 0.66 that would be obtained for flow down a channel between two vertical plates.

Mass fluxes through the Salt Wash Canyon, computed from wind profile, valley width, and air density data, assuming $a = 0.7$, using the expression given as the first term in (6), were directed out of the basin after 2000 MST and attained an evening near-steady-state value of 1.7 kton s^{-1}. The compensatory subsidence at the control volume lid, computed by solving (6) for vertical velocity, was at the mean rate of 0.026 m s^{-1} (Fig. 10). This mean subsidence occurs at a time when the top of the basin inversion is rising at the rate of about 100 m h^{-1} or 0.028 m s^{-1}.

The control volume contained 23.8 km^3 of air at a density of about 0.97 kg m^{-3} so that, at a mass removal rate of 1.7 kton s^{-1}, the basin mass turnover time would be 3.8 h. For comparison, the turnover time for Colorado's Brush Creek Valley is about 3–3.5 h, as derived from Clements et al.'s (1989) and Whiteman and Barr's (1986) volume flux estimates and using King's (1989) Doppler lidar-derived correction factor to account for cross-valley variation of wind speed.

5. Evaluation of the basin heat budget

The methods for evaluating the individual terms of (4) are discussed in this section and the results are shown in Fig. 11. Results are presented primarily for the evening period between 1900 and 2400 when both tethered balloon systems were in operation.

a. Term A: Rate of increase of heat storage

The rate of increase of heat storage is given by

$$\underbrace{\iiint \bar{\rho} c_p \frac{\partial \bar{\theta}}{\partial t} dv}_{\text{A}} = \int_0^h \bar{\rho} c_p \frac{\partial \bar{\theta}}{\partial t} A_{xy}(z) dz \quad (\text{W}), \tag{7}$$

where $A_{xy}(z)$ is the horizontal basin drainage area at height z obtained from Fig. 4. The mean density and the time rate of change of potential temperature were determined from sequential tethered balloon soundings at the basin site and were assumed horizontally invariant within the basin. These assumptions are expected to produce a reasonable approximate value of term A since buoyancy forces tend to produce horizontal stratification in the stable air mass within the basin, and the confined terrain protects the pool from perturbation by external flows. We note, however, that the rate of change of potential temperature in the shallow slope flow layer will be higher than over the basin center during the brief period when the slope flow layer first starts to form in the late afternoon or early evening. The effect of this on the heat budget is mitigated, somewhat, by the shallowness of the slope flow layers when compared to the volume of the basin control volume.

The normalized value of term A averaged −61 W m^{-2} during the evening but varied between −46 and −95 W m^{-2}. The negative values represent a loss of heat storage from the basin atmosphere. This nighttime rate of heat loss in the Sinbad Basin is larger than the values of −10 to −25 reported in the Brush Creek

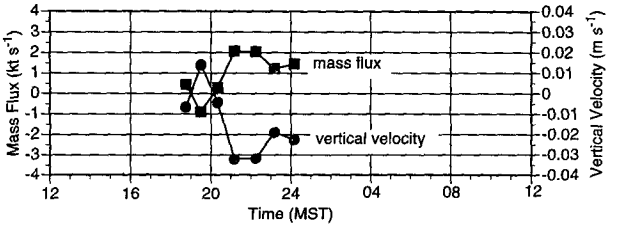

FIG. 10. Mass flux through the Salt Wash Canyon below the control volume lid (squares) and the corresponding mean vertical velocity over the lid of the control volume (dots).

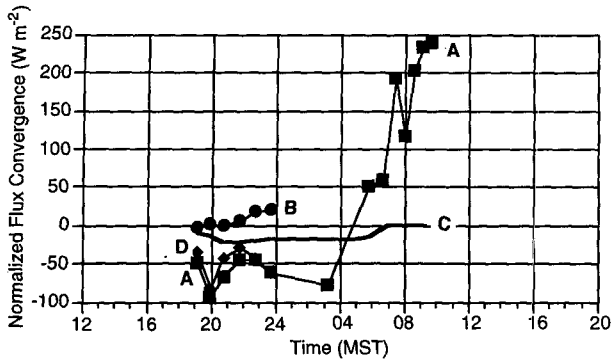

FIG. 11. Components of the Sinbad Basin atmospheric heat budget on 15–16 July 1988. All heat budget terms are normalized by the drainage area of the basin. Term A is the rate of increase of heat storage, term B is the convergence of mean potential temperature flux, term C is the radiative flux convergence, and term D is the convergence of turbulent sensible heat flux calculated as a residual in the atmospheric heat budget.

Valley by Horst et al. (1987, 1989) and larger than the value of -46 W m^{-2} reported for the Aizu Basin by Kondo et al. (1989).

b. *Term B: Convergence of mean potential temperature flux*

Using the divergence theorem, the convergence of mean potential temperature flux by the mean wind can be expressed in terms of the fluxes through the two open boundaries of the control volume, as follows:

$$\iint -\bar{\rho} c_p \mathbf{n}\cdot\bar{\mathbf{V}}\,\bar{\theta}\,dA = \iint -\bar{\rho} c_p \bar{u}\,\bar{\theta}\,dA_{yz} + \iint -\bar{\rho} c_p \bar{w}\,\bar{\theta}\,dA_{xy}(h) \quad \text{(W)}. \quad (8)$$

The boundary fluxes in (8) were approximated by the expression

$$\underbrace{\iint -\bar{\rho} c_p \mathbf{n}\cdot\bar{\mathbf{V}}\,\bar{\theta}\,dA}_{\text{B}} \approx \underbrace{\int -\bar{\rho} c_p a \bar{u}_c(z)\bar{\theta}(z)b(z)\,dz}_{\text{E}} + \underbrace{-\langle\bar{\rho}\rangle_h c_p \langle\bar{w}\rangle_h \langle\bar{\theta}\rangle_h A_{xy}(h)}_{\text{F}} \quad \text{(W)}, \quad (9)$$

where density and potential temperature in term E were determined from the Salt Wash balloon soundings. In evaluating term F in (9), we have assumed that the individual terms in the integrand can be replaced by their average values across the basin lid. This allows us to use the mean vertical velocity obtained from the mass budget and the θ value obtained from our soundings. We discuss the limitations of this approximation further below, and in Part II of this paper we use a numerical model to examine this question more fully.

Terms E and F of (9) can be compared with the two terms of the mass budget equation (6). From the mass budget we know that positive (negative) values of u result in negative (positive) values of w. Since all other variables in terms E and F are positive, terms E and F will have opposite signs. Further, in a down-valley flow in a stable atmosphere where potential temperature increases with height and is horizontally homogeneous at height $z = h$, term E is expected to be smaller in magnitude than term F. This is apparent because the canyon-cross-section-weighted value of potential temperature will certainly be less than the average value of potential temperature at the top of the basin control volume. Then (9) will be positive and term B will produce warming in the basin.

Calculations show that normalized evening values of term B are 7 ± 9.3 W m^{-2} (i.e., mean plus/minus standard deviation). Term B, as shown above, is computed as the sum of terms E and F. These terms have large magnitudes (approximately 500 GW; i.e., normalized values of about 7200 W m^{-2}) and are of opposite sign. Because term F is larger than term E, the small difference between the two terms is constrained to be a positive number when the winds blow down-valley.

Because of unsupported assumptions required in the calculation of term B using limited observational data and its evaluation as a difference between two large values, the accuracy of the mean flux term is quite uncertain and its evaluation in this way is one of the key drawbacks of the observational method of evaluation of the heat budget equation. The continuity equation, however, couples terms E and F, and under- or overestimates of mass flux through the Salt Wash will be compensated by under- or overestimates of mass subsidence over the basin. Equation (9) clearly will be sensitive to potential temperature and density differences between the two control surfaces. An error of 0.4 K in $\theta(h)$ results in an error of 8 W m^{-2} for the normalized value of term B. The density error produced by a pressure offset of 1 hPa between the two tethered balloon sounding systems would also produce an error of 8 W m^{-2}.

The mean flux divergence term has an important effect on the nighttime meteorology of valleys and basins because it introduces warm air, which regulates the down-valley wind system, into the valley atmosphere. The near-steady-state down-valley wind that is attained in many valleys in late evening requires that the horizontal pressure gradient built up hydrostatically between valley and plain be maintained. The down-valley winds, however, carry cooled air out of the valley and this cooled air is replaced by warm air from above. The replacement air must be cooled within the valley in order to maintain the down-valley flow. A steady-state wind thus represents a dynamic balance between the

rate of input of warm air and the cooling power of the valley. The nighttime down-canyon winds, according to valley wind theory (Wagner 1938), require a temperature gradient between air within the basin and air outside the basin. Observations at the level of the control volume lid show that the temperature gradient is in the correct direction (Fig. 12), with potential temperatures about 0.8 K warmer above the Salt Wash site.

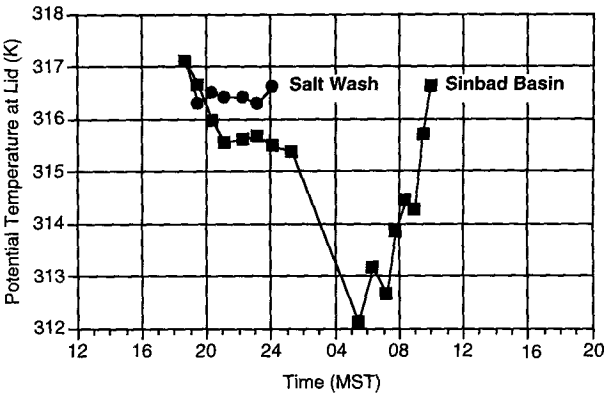

FIG. 12. Potential temperature as a function of time at the control volume lid at the two tethered balloon sites.

c. Term C: Radiative flux convergence

The radiative flux convergence term can be rewritten as

$$\underbrace{\iiint -\left(\frac{\theta}{T}\right)\nabla\cdot\mathbf{R}\,dv}_{\mathrm{C}} \approx -\left(\frac{\theta}{T}\right)_m \iint \mathbf{n}\cdot\mathbf{R}\,dA \quad (\mathrm{W}), \tag{10}$$

where the factor in parentheses on the right-hand side, evaluated at the mean pressure of the Sinbad Basin (808 hPa), is 1.06.

Radiation calculations were made with Cox et al.'s (1976) broadband longwave radiative transfer model for a plane-parallel atmosphere, accounting for collision broadening. Calculations were made for each of the Sinbad tethered balloon sounding times using tethered balloon profiles of temperature and moisture for the lower levels, using sondes launched from the basin floor for intermediate levels, and using rawinsondes from Grand Junction, Colorado, for heights above the 530-hPa pressure level. Grand Junction is 76 km north-northeast of the Sinbad Basin and observations were available there at 0415 and 1615 MST. Time interpolations were performed from the observations at the intermediate and upper levels. The carbon dioxide mixing ratio was assumed to be 0.501 g kg^{-1} and independent of elevation. Ozone concentrations and temperature profiles above 100 hPa were obtained from a mid-latitude climatological summary (McClatchey et al. 1972). The variable high thin cloudiness was simulated in the radiative transfer model by specifying a cloud at 470–480 hPa, as suggested by the presence of a moist layer in the Grand Junction sounding. Radiative transfer calculations were made for both cloudy and clear atmospheres. Radiative flux divergences (RFDs) over the control volume depth did not vary greatly between the two atmospheres (typical difference of 7 W m^{-2}) so that RFDs for the control volume were estimated by interpolating linearly between modeled RFDs for the two atmospheres on the basis of the observed and two model-calculated values of surface net radiation.

The normalized value of term C averaged over all the soundings was -18.5 ± 4.7 W m^{-2} for the evening period (Fig. 11). These negative flux convergences (i.e., divergences) produce cooling in the basin atmosphere. The longwave radiative flux convergence increased following sunrise to attain about -5 W m^{-2}. Other investigators (e.g., Hennemuth 1985) have calculated small shortwave radiative flux convergences during daytime that act to balance the longwave flux divergence. Thus, the daytime all-wave RFD plotted in Fig. 11 is assumed negligible.

d. Term D: Convergence of turbulent sensible heat flux

Term D was evaluated from (4) as a heat budget residual, obtaining normalized values of -49.5 ± 19.4 W m^{-2} (Fig. 11). These negative values of turbulent sensible heat flux convergence are necessary to produce the observed cooling in the control volume. In the following section we compare these values to sensible heat flux estimates made for the basin floor using surface energy budget measurements.

e. Estimation of sensible heat flux at the basin floor

The surface turbulent sensible heat flux was evaluated at the basin site by means of the surface energy budget equation

$$-Q^* = Q_H + Q_E - Q_G \quad (\mathrm{W\ m^{-2}}), \tag{11}$$

where Q^* is net radiation, Q_G is soil heat flux, Q_H is the sensible heat flux, and Q_E is the latent heat flux. All fluxes are positive when directed upward.

The terms in (11) were evaluated as follows. Latent heat flux was assumed negligible in the arid basin, net radiation was evaluated directly from measurements, and soil heat flux was calculated from

$$Q_G = -\int_{-d}^{0} C\frac{\partial T}{\partial t}\,dz + K\frac{\partial T}{\partial z}\bigg|_{z=-d} \quad (\mathrm{W\ m^{-2}}), \tag{12}$$

where T is soil temperature (°C), t is time (s), z is height above the soil surface (m), C is volumetric

heat capacity (J m^{-3} K^{-1}), K is soil conductivity (W m^{-1} K^{-1}), and d is the base of the soil column.

The integral in (12) was calculated in finite difference form using the layer depths and heat capacities given in Table 1 and the observed soil temperature profiles (Fig. 9). The layer heat capacities in the table were determined as a weighted average of the tabulated volumetric heat capacities of the soil constituents (Hillel 1982) using moisture content, volume fraction, and bulk density values determined from laboratory analyses of soil samples. The last term in (12) is a relatively small term that corrects the first term for the heat flux in or out of the base of the soil column. It was estimated as the product of the measured soil temperature gradient at the lowest two soil thermocouples and a model-derived estimate of soil conductivity. The model, described by Hanks and Ashcroft (1980), used an explicit backward finite-difference procedure, in which the temperatures at −0.24 and −1.05 m were the boundary conditions and the procedure was to determine the soil conductivity that provided the best agreement between measured and modeled soil temperatures at the −0.50-m level over the course of 36 hours centered within the experimental period. This model-calculated conductivity (0.95 W m^{-1} K^{-1}) was assumed representative of the base of the soil column. The soil temperature gradient between −0.50 and −1.05 m (about 6 K m^{-1}) varied only slightly during the experimental period, and this gradient was assumed to be representative of the base of the soil column so that evaluation of the last term in (12) produced an average rate of loss of 6 ± 0.4 W m^{-2} out the base of the soil column.

Time series plots of net radiation, soil heat flux, sensible heat flux, and extraterrestrial solar radiation at the basin site are shown for both nighttime and daytime in Fig. 13.

During nighttime (1935 through 0515 MST), the upward flux of heat from the soil at the basin site, as calculated above, was 69 ± 29 W m^{-2}. Net radiation during this period was 62 ± 5 W m^{-2}. Thus, the upward soil heat flux slightly overcompensated the nocturnal radiative loss on the basin floor. From (11), the sum of sensible and latent heat fluxes must have been near zero or slightly positive (i.e., a flux of heat into the atmosphere) at this site. Any appreciable sensible and latent heat fluxes would have to be in opposite directions. Significant evaporation could be supported if the sensible heat flux could be maintained—for example, through the so-called oasis effect (Miller 1965). But it is nighttime when plant stomates are closed, no deep-rooted plant species are present at this site, and the soil is very dry. Further, no condensation was detected on the soil or grasses at this site and the atmospheric humidity budget showed little change in basin humidity levels. We conclude that both the latent and sensible heat fluxes are small at the basin floor at nighttime. Our atmospheric heat budget computations show high rates of energy loss from the basin atmosphere during the night that cannot be supported solely by radiative flux divergence. Therefore, we must also conclude, in agreement with previous investigators (e.g., Maki et al. 1986), that sensible heat fluxes on the basin floor are unrepresentative of the basin as a whole and that much higher downward sensible heat fluxes must occur over the sidewalls where downslope flows produce the necessary wind shear and turbulence. Note that even if we have substantial errors in our evaluation of term B, because that term should be positive, our conclusions regarding the relative contributions of sensible heat fluxes over the basin floor and sidewalls will remain valid. Further evidence for our conclusions is provided by numerical simulations, which are described in Part II of this paper.

TABLE 1. Calculated volumetric soil heat capacities.

Layer	Depth (m)	C (MJ m^{-3} K^{-1})
1	0.000–0.054	1.37
2	0.054–0.113	1.60
3	0.113–0.239	1.72
4	0.239–0.502	1.74
5	0.502–1.054	1.72

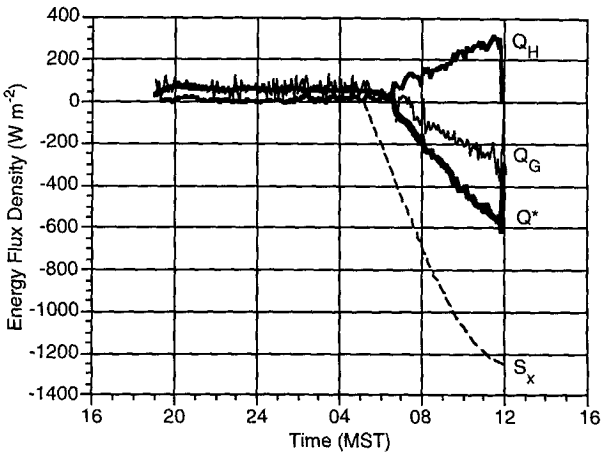

FIG. 13. Components of the surface energy balance at the basin site on 15–16 July 1988: S_x is extraterrestrial solar radiation, Q^* is net radiation, H is sensible heat flux, and Q_G is soil heat flux. Upward fluxes are positive. Nighttime values of Q_G and H at this site are not representative of the basin as a whole (see text).

During daytime, much of the net radiation goes into sensible heat flux initially, but both the ground and the atmosphere receive large amounts of energy. By noon, both the atmosphere and the ground are receiving energy at the rate of nearly 300 W m^{-2}.

6. Evaluation of the basin humidity budget

Since no clouds formed or dissipated within the basin during the experimental period, the change of water

vapor storage in the basin atmosphere was produced solely by vapor convergence caused by differential mean and/or turbulent vapor fluxes through the basin boundaries. This can be expressed by rewriting (5) using the divergence theorem to obtain

$$\underbrace{\iiint \bar{\rho}\frac{\partial \bar{q}}{\partial t}\,dv}_{\text{G}} = \underbrace{\iint -\bar{\rho}\bar{\mathbf{V}}\bar{q}\,dA}_{\text{H}} + \underbrace{\iint -\bar{\rho}\overline{V'q'}\,dA}_{\text{I}} \quad (\text{kg s}^{-1}). \quad (13)$$

Term H, since the wind velocity perpendicular to the solid boundaries of the basin volume (basin floor and sidewalls) is zero, involves only vertical fluxes through the basin lid and horizontal fluxes through the vertical basin outflow cross section and can be evaluated as

$$\underbrace{\iint -\bar{\rho}\bar{\mathbf{V}}\bar{q}\,dA}_{\text{H}} \approx \underbrace{\int -\bar{\rho}a\bar{u}(0,z)\bar{q}(z)b(z)dz}_{\text{J}} + \underbrace{-\langle\bar{\rho}\rangle_h\langle\bar{w}\rangle_h\langle\bar{q}\rangle_h A_{xy}(h)}_{\text{K}} \quad (\text{kg s}^{-1}). \quad (14)$$

Term I represents the turbulent moisture fluxes across the volume boundaries. At the basin floor and sidewalls this represents evaporation or condensation of moisture at the surface. At the open surfaces of the volume this represents turbulent fluxes on timescales shorter than the averaging time of the mean fluxes.

Because there were no direct measurements of turbulent moisture fluxes, we take the approach of determining turbulent moisture flux convergence as a residual from (13) after calculating the change of moisture storage and the flux of moisture by the mean wind. The results are shown in Fig. 14. The basin atmosphere generally dried during nighttime and moistened during daytime. Between 2100 and 0630 MST, the rate of drying was nearly constant at about 0.5 ton s^{-1}, and the mean mixing ratio of the basin atmosphere during this period decreased by about 0.76 g kg^{-1}. The convergence of moisture flux by the mean wind was small during the night (0.002 ± 0.114 ton s^{-1}), so that the nighttime changes in moisture storage are attributed primarily to turbulent moisture flux divergence. This divergence was small, however, and if it were represented entirely by condensation on the basin floor and sidewalls, it would result in a dew deposition rate of only 2.6×10^{-5} mm h^{-1} m^{-2}. After sunrise on 16 July the rate of increase of moisture storage in the basin

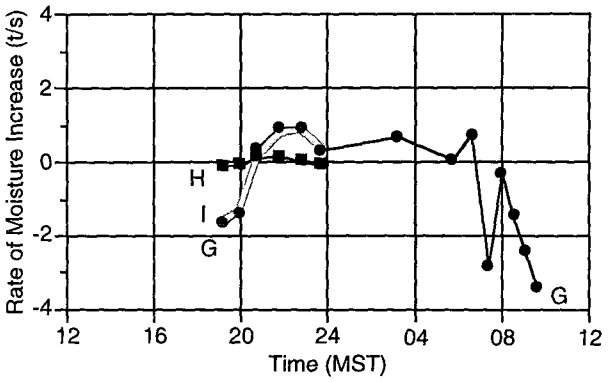

FIG. 14. Rates of moisture increase in the basin atmosphere due to the various terms in the humidity budget. Terms include (G) change of moisture storage, (H) moisture flux convergence by mean flow, and (I) turbulent moisture flux convergence.

atmosphere rose substantially, attaining rates of over 3 ton s^{-1} by 1000 MST. Since dual tethered balloon measurements were not available during this time we cannot determine the relative contributions of mean and turbulent moisture flux convergences.

Hennemuth and Neureither's (1986) investigation of the moisture budget of Switzerland's Dischma Valley pointed out that the upslope flows export humidity from the valley during the morning, that evaporation humidifies the valley during daytime, and that the onset of the up-valley wind transports humidity into the valley in the afternoon. The Sinbad Basin is in a very different humidity and topographic regime. Here, according to observations from a single day, a weak dewfall or turbulent flux out the top of the basin decreases the humidity marginally during nighttime, and the down-canyon winds make almost no contribution to the moisture budget. The moisture in the basin atmosphere increases during daytime, but the relative roles of the up-canyon flows and local evaporation cannot be determined.

7. Discussion

The Sinbad Basin was selected for the experiments partially because of expectations that the basin outflow would be weak. The observations show, however, that the mass flux through the narrow Salt Wash Canyon is substantial—similar to fluxes through the well-drained Brush Creek Valley. We hypothesize that this is caused by the strong horizontal pressure gradient that develops between a basin and its surroundings due to cooling within the basin. Naturally the steady-state flow that is eventually attained depends also on turbulent shear stresses in the outflow canyon.

Some uncertainties are introduced into our evaluation of the atmospheric heat budget because of the assumptions necessary to close the budget. These assumptions include the horizontal homogeneity assumption in term A, the integration approximation as-

sumption in term B, and the plane-parallel atmosphere assumption used to evaluate term C. The resultant heat budget computations show that large sensible heat flux divergences must occur from the basin control volume during nighttime despite calculations of negligible turbulent sensible heat flux at the basin floor. This suggests that correspondingly stronger downward turbulent sensible heat fluxes must occur in the downslope drainage flows over the basin sidewalls—a conclusion reached by previous investigators (Kondo et al. 1989; Maki et al. 1986) and supported by the numerical experiments described in Part II. The Sinbad Basin control volume lid is below the highest terrain on the west and north sides of the basin, so that one might also expect a significant component of upward turbulent sensible heat flux along these edges of the control volume lid caused by the downslope flow of cold air off the higher terrain. The partitioning of this heat transfer into mean and turbulent energy budget components is problematical, as the shallow drainage flows are not resolved in our calculation of the mean flux divergence. There is undoubtedly a mean sinking of cold air near the slopes at the control volume lid.

The net radiation and soil heat flux measurements on the basin floor were obtained on a nonsloping, largely unvegetated, sandy soil surface that, while reasonably representative of the basin floor, is not representative of the basin as a whole. The rim of the basin is exposed sandstone, and 70% of the basin (Fig. 1) is covered with shrubs (e.g., sagebrush) and a mixed forest of widely dispersed pinyon pine and juniper. We speculate that the enhanced downward turbulent heat flux on the valley sidewalls may be produced partially by the sidewall vegetation. The production of shear generated turbulence by the flow of air around the vegetation is well known, but here we refer to aspects of the surface energy balance. We have seen from the observations on the basin floor that net outgoing radiation loss is countered at night by a large upward soil heat flux. The energy balance of a tree or shrub, however, may involve the same nighttime net outgoing radiation (e.g., at the top of the canopy), but the trunks, stems, and needles or leaves are poor conductors of heat to the soil, so that the outgoing radiation is not countered by a ground conduction–like term and must be balanced by sensible (or latent) heat flux. The sensible heat is transferred from the atmosphere to the leaves or needles, reducing the heat stored in the atmosphere, and this process is further facilitated by the flow of air through the canopy. Similarly, during daytime, net radiation on the canopy is balanced by sensible (and latent) heat flux, and the shadows cast on the ground reduce the soil heat flux and its corresponding release during nighttime. It would clearly be useful to conduct further experiments to investigate the role of sidewall vegetation on surface sensible heat flux.

The high rate of heat loss from the basin atmosphere through the night can be attributed partially to the small air volume in the basin atmosphere relative to an equal-depth atmosphere over a plain, given the same surface areas at the volume tops. This geometric effect can be illustrated for the basin by considering a surface turbulent sensible heat flux $H_0 = \bar{\rho} c_p \overline{w'\theta'_0}$ expressed per unit of projected horizontal surface area over the basin watershed. If the horizontal turbulent fluxes and the vertical turbulent flux above the basin were negligible, a balance between terms A and D in (4) would result in

$$\underbrace{\iiint \bar{\rho} c_p \frac{\partial \bar{\theta}}{\partial t}\, dv}_{\text{A}} = \underbrace{H_0 A_{xy}(h)}_{\text{D}} \quad \text{(W)}, \quad (15)$$

from which the average rate of change of potential temperature in the volume could be expressed as

$$\overline{\frac{\partial \bar{\theta}}{\partial t}} = \frac{H_0}{\bar{\rho} c_p} \frac{A_{xy}(h)}{v} \quad (\text{K s}^{-1}). \quad (16)$$

The rate of change of potential temperature in a basin (or valley) atmosphere is then seen to depend on the ratio of the drainage area at the basin's top to the atmospheric volume enclosed by the basin (Steinacker 1984; McKee and O'Neal 1989). Because the atmospheric volume is reduced in the basin due to the sloping sidewalls, a given basin drainage area will enclose less volume than an equal-depth drainage area over a plain. An equal heat input to (or extraction from) the two volumes will produce higher warming (or cooling) rates in the smaller volume. The geometric factor, defined as the area to volume ratio for the valley divided by the area to volume ratio for a plain, has been called a *topographic amplification factor* (Whiteman 1990) since its effect is to produce a greater diurnal temperature range in the valley or basin than over an adjoining plain. It is this difference in diurnal temperature ranges that produces the well-known diurnal wind systems. The resulting winds act to equalize horizontal pressure gradients developed hydrostatically between basin and plain. Data from Fig. 4 can be used to calculate the area to volume ratio for the Sinbad Basin. For the control volume this ratio is 1.52 times the similar ratio for a plain and implies that nighttime cooling rates and daytime heating rates in the basin will be significantly enhanced relative to a plain. Enhanced basin cooling rates that may be attributable to the topographic amplification factor have been reported by previous investigators (e.g., Sauberer and Dirmhirn 1954, 1956; Petkovsek 1973).

We have shown that the Sinbad Basin and Brush Creek Valley mass fluxes are comparable. Since the well-studied Brush Creek Valley is located only 125 km northeast of the Sinbad Basin and is in a similar climate setting, it is useful to compare the energetics of the Sinbad Basin with the Brush Creek Valley and with

TABLE 2. Summary of heat budget terms (W m^{-2}). The last line shows the measured surface sensible heat flux on or near the floor of the valley or basin.

Valley/basin	Term	Sinbad Basin	Brush Creek Valley	Brush Creek Valley	Aizu Basin
Date		15 July 1988	26 September 1984	30 September 1984	October, May
Source		—	Horst et al. (1989)	Horst et al. (1989)	Kondo et al. (1989)
Storage	A	−61	−10	−25	−46
Advection	B	7	31	77	0*
Radiation	C	−18.5	−7	−8	−9
Sensible heat	D	−49.5	−34	−94	−37
Sensible heat measured	Q_H	7	−18	−33	0

* This term was assumed to be negligible.

other valleys and basins for which data are available. This is done for individual terms of the heat budget in Table 2.

A convenient way of comparing the energetics of multiple valleys and basins is to cast the budget terms in a dimensionless form. We begin with the heat budget equation in the form A = B + C + D, with the terms defined as in (4). Terms C and D represent the driving terms of the heat budget. The relative importance of C and D, and their sum, depends on the climate setting of the valley, soil moisture, vegetation cover, albedo, and other factors. Rearranging the equation and dividing by (C + D) results in the equation

$$\frac{A}{C+D} - \frac{B}{C+D} = 1. \qquad (17)$$

The two terms on the left-hand side of this equation add to 1 and provide basic measures of the disposition of radiative and turbulent sensible heat flux divergence into changes of heat storage or advection. The energetics of a particular valley or basin can thus be summarized by locating the valley's position on the line defined by (17) and shown in Fig. 15, as we have done for the valleys listed in Table 2. Valleys that are well-drained at night cannot cool strongly throughout the night and eventually must approach a steady-state temperature. They are thus located on the right end of the line. The flow of heat into trapped valleys or basins, on the other hand, leads to strong cooling and little advective warming. Basins are thus found on the left end of the line.

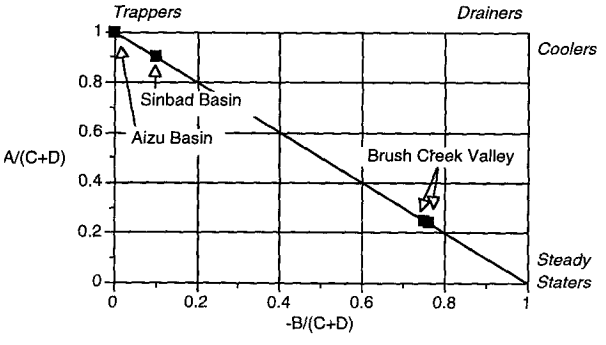

FIG. 15. Categorization of valleys and basins with respect to the ratio of selected heat budget terms. The advection term for the Aizu Basin was assumed to be zero.

8. Conclusions

A meteorological field experiment was conducted in Colorado's arid Sinbad Basin on 15–16 July 1988 beginning in the late afternoon. The evolution of vertical temperature structure over the center of the basin during the evening was characterized by the upward growth of a stable boundary layer from the floor of the basin, with little cooling above the stable boundary layer. Winds were weak within the growing stable boundary layer.

The Sinbad Basin atmosphere cooled strongly and continuously during the night. This is in contrast to well-drained valleys, which attain small equilibrium cooling rates once the down-valley wind system becomes well established. The small equilibrium cooling rates in valleys are caused by the sinking of warm air into the valleys to replace air that has been cooled within the valleys and removed by the down-valley wind system. The basin atmosphere cools strongly because heat losses due to turbulent sensible heat flux divergence and radiative flux divergence are not countered by the strong subsidence warming that is a feature of well-drained valleys.

To test this hypothesis we evaluated mass, heat, and moisture budget equations for the basin atmosphere using tethered balloon, airsonde, and surface energy budget measurements focused primarily on the evening period. The Sinbad Basin has a particularly simple drainage region, a single narrow exit canyon, and a climate setting where latent heat fluxes are small. Evaluations were made in a control volume bounded by the floor and sidewalls of the basin so that only two surfaces of the control volume, the horizontal lid and the vertical cross section normal to the exit canyon, were open to airflows. These factors were expected to sim-

plify the computation of some of the budget terms compared to open control volumes over plains.

Evaluation of the mass budget equation using observations showed that the nocturnal drainage through the narrow exit canyon produced a mean mass flux from the basin of 1.7 kton s^{-1}. From the mass continuity equation, this outflow required a compensatory subsidence of air into the basin at the mean rate of 0.026 m s^{-1}. The drainage flow was produced by a strong horizontal pressure gradient that developed hydrostatically between the cool air inside the basin and the warmer air outside the basin.

The terms of the nocturnal heat budget can be expressed as the heat flux convergence into the basin volume per unit area at the basin's top in units of watts per square meter. At night, cold air drained out of the basin through the narrow canyon, causing warmer air to subside into the basin and producing a net warming at the rate of 7 W m^{-2}. Observations showed a net nighttime cooling of the basin atmosphere at the rate of 61 W m^{-2}. Radiative flux divergence accounted for a cooling of 18.5 W m^{-2}, and thus sensible heat flux divergence, calculated as a residual, must produce a cooling of 49.5 W m^{-2}. A discrepancy was found between this calculated sensible heat flux divergence for the basin as a whole and the sensible heat flux divergence estimated from surface energy budget measurements on the basin floor, where the surface sensible heat flux was near zero. This suggests, as other investigators have pointed out, that turbulence in the sidewall drainage flows must play an important role in providing the required turbulent sensible heat flux divergence. The effect of the sidewall vegetation on the generation of turbulence and on the surface energy budget is another factor that may be significant on the sidewalls.

The basin atmospheric moisture budget during the experimental period is characterized by slight moistening during daytime and weak drying during nighttime. The nighttime mean moisture flux downward into the basin at its top is matched closely by the mean horizontal flux of moisture out the basin exit, so that the moistening (drying) is produced by turbulent moisture flux convergence (divergence) into the basin atmosphere.

A dimensionless form of the heat budget equation was used to compare the energetics of different valleys and basins using the Sinbad Basin results and published information for other valleys. By using this form of the heat budget equation, valley and basins are classified with respect to their response to radiative and turbulent sensible heat divergences. In well-drained valleys much of the heat divergence is countered by subsidence warming so that the atmosphere cools only weakly with time. Basins, sinkholes, or other confined terrain with weaker drainage wind systems are generally characterized by stronger cooling rates.

The many assumptions required to evaluate the budget terms in the Sinbad Basin with the available data are documented, and the uncertainties introduced by these assumptions are considered a drawback to the present method. The evaluation of mean advection terms is also troublesome because they are calculated as small differences between large quantities. An alternative method for evaluating the budget equations with a dynamic model eliminates the need for these restrictive assumptions since conservation equations are automatically satisfied in the model formulations. Additional issues arise, however, regarding the suitability of turbulence parameterizations and digital elevation data and the matching of observed wind and temperature profiles. An evaluation of the mass and heat budget equations for the Sinbad Basin is presented using a dynamic model in the accompanying Part II paper by Fast et al. (1996). The dynamic model results are qualitatively in agreement with those given here. Although the magnitudes of the individual budget terms differ, the conclusions regarding the signs, relative magnitudes of the budget terms (except for the advection term), and the importance of sensible heat fluxes over the slopes compared to those over the basin floor are essentially the same in the two studies.

In future work, experiments should be conducted to investigate valley and basin energetics in other climatological and topographic settings and to investigate the effects of sidewall vegetation. Observational studies in frost hollows, sinkholes, or other nondraining basins would provide important additional information on cases when the advective terms become small.

Acknowledgments. Mr. John Hubbe and Dr. Bill Pennell of Pacific Northwest National Laboratory assisted in the collection of data at the basin site. John Kleist and Tom Merrill of Colorado State University collected the Salt Wash tethered balloon data. Dr. Markus Furger and Dr. Werner Eugster made useful comments on early versions of the manuscript. The manuscript was finished while one of the authors (CDW) was a visiting scientist at the University of Berne and he wishes to thank Dr. Heinz Wanner for arranging this appointment.

This research was supported by the U.S. Department of Energy's Environmental Sciences Division under Contract DE-AC06-76RLO 1830 with Pacific Northwest National Laboratory as part of their Atmospheric Studies in Complex Terrain program. Pacific Northwest National Laboratory is operated by Battelle Memorial Institute for the U.S. Department of Energy.

REFERENCES

Barnes, F. A., 1978: *Canyon Country Geology.* Wasatch Publishers, 156 pp.

Clements, W. E., J. A. Archuleta, and D. E. Hoard, 1989: Mean structure of the nocturnal drainage flow in a deep valley. *J. Appl. Meteor.*, **28,** 457–462.

Cox, S. K., M. C. Polifka, K. Griffith, A. Rockwood, and D. Starr, 1976: Radiative transfer computational routines for atmospheric science applications. CSU-ATS Research Rep., Atmospheric Science Department, Colorado State University, Fort Collins, CO, 75 pp.

Fast, J. D., S. Zhong, and C. D. Whiteman, 1996: Boundary layer evolution within a canyonland basin. Part II: Numerical simulations of nocturnal flows and heat budgets. *J. Appl. Meteor.*, **35,** 2162–2178.

Freytag, C., 1985: MERKUR-results: Aspects of the temperature field and the energy budget in a large alpine valley during mountain and valley wind. *Contrib. Atmos. Phys.*, **58,** 458–476.

——, 1987: Results from the MERKUR experiment: Mass budget and vertical motions in a large valley during mountain and valley wind. *Meteor. Atmos. Phys.*, **37,** 129–140.

Hanks, R. J., and G. L. Ashcroft, 1980: *Applied Soil Physics.* Springer-Verlag, 159 pp.

Hennemuth, B., 1985: Temperature field and energy budget of a small Alpine valley. *Contrib. Atmos. Phys.*, **58,** 545–559.

——, 1986: Thermal asymmetry and cross-valley circulation in a small alpine valley. *Bound.-Layer Meteor.*, **36,** 371–394.

——, and U. Köhler, 1984: Estimation of the energy balance of the Dischma Valley. *Arch. Meteor. Geophys. Bioklimatol. Ser. B,* **34,** 97–119.

——, and I. Neureither, 1986: Das Feuchtefeld in einem alpinen Endtal. (The humidity field in an alpine end valley). *Meteor. Rundsch.*, **39,** 233–239.

Hillel, D., 1982: *Introduction to Soil Physics.* Academic Press, 364 pp.

Horst, T. W., K. J. Allwine, and C. D. Whiteman, 1987: A thermal energy budget for nocturnal drainage flow in a simple valley. *Preprints, Fourth Conf. on Mountain Meteorology,* Seattle, WA, Amer. Meteor. Soc., 15–19.

——, D. C. Bader, and C. D. Whiteman, 1989: Comparison of observed and simulated nocturnal valley thermal energy budgets. *Preprints, Int. Conf. on Mountain Meteorology and ALPEX,* Garmisch-Partenkirchen, Germany, German Meteor. Soc. 127.

King, C. W., 1989: Representativeness of single vertical wind profiles for determining volume fluxes in valleys. *J. Appl. Meteor.*, **28,** 463–466.

Kondo, J., T. Kuwagata, and S. Haginoya, 1989: Heat budget analysis of nocturnal cooling and daytime heating in a basin. *J. Atmos. Sci.*, **46,** 2917–2933.

Maki, M., T. Harimaya, and K. Kikuchi, 1986: Heat budget studies on nocturnal cooling in a basin. *J. Meteor. Soc. Japan,* **64,** 727–740.

McClatchey, R. A., R. W. Fenn, J. E. A. Selby, S. E. Voltz, and J. S. Garing, 1972: Optical properties of the atmosphere. 3d ed. AFCRL-72-0497, Air Force Cambridge Research Laboratory, L. G. Hanscom Field, Bedford, MA.

McKee, T. B., and R. D. O'Neal, 1989: The role of valley geometry and energy budget in the formation of nocturnal valley winds. *J. Appl. Meteor.*, **28,** 445–456.

Miller, D. H., 1965: The heat and water budget of the earth's surface. *Adv. Geophys.*, **11,** 175–301.

Petkovsek, Z., 1973: Vergleichungen der lokalen Temperaturänderungen im Gebirgsgebiete, Flachland und freie Atmosphäre (Comparison of local temperature variations in a mountainous region, on a plain, and in the free atmosphere). *La Météorologie,* **10–11,** 135–150.

Sauberer, F., and I. Dirmhirn, 1954: Über die Entstehung der extremen Temperaturminima in der Doline Gstettner-Alm. (On the occurrence of extreme temperature minimums in the Gstettner-alm sinkhole). *Arch. Meteor. Geophys. Bioklimatol. Ser. B,* **5,** 307–326.

——, and ——, 1956: Weitere Untersuchungen über die kaltluftansammlungen in der Doline Gstettner-Alm bei Lunz in Niederösterreich (Further studies of the collection of cold air in the Gstettner-Alm sinkhole near Lunz in lower Austria). *Wetter Leben,* **8,** 187–196.

Steinacker, R., 1984: Area-height distribution of a valley and its relation to the valley wind. *Contrib. Atmos. Phys.*, **57,** 64–71.

Vergeiner, I., E. Dreiseitl, and C. D. Whiteman, 1987: Dynamics of katabatic winds in Colorado's Brush Creek Valley. *J. Atmos. Sci.*, **44,** 148–157.

Wagner, A., 1938: Theorie und Beobachtung der periodischen Gebirgswinde. (Theory and Observation of Periodic Mountain Winds). *Gerlands Beitr. Geophys.*, **52,** 408–449. (English translation: Whiteman, C. D., and E. Dreiseitl, 1984: Alpine Meteorology: Translations of Classic Contributions by A. Wagner, E. Ekhart, and F. Defant. PNL-5141/ASCOT-84-3, Pacific Northwest Laboratory, Richland, WA, 121 pp.)

Whiteman, C. D., 1990: Observations of thermally developed wind systems in mountainous terrain. *Atmospheric Processes over Complex Terrain, Meteor. Monogr.*, No. 45, Amer. Meteor. Soc., 5–42.

——, and S. Barr, 1986: Atmospheric mass transport by along-valley wind systems in a deep Colorado valley. *J. Climate Appl. Meteor.*, **25,** 1205–1212.